# Dynamic Analysis of a Beam with Additional Auxiliary Mass Spatial Via Spectral Element Method

**E. U. L. Palechor, M. R. Machado, M. V. G. de Morais and L. M. Bezerra**

**Abstract** This paper aims to propose a new spectral element with additional mass. Methodologies for structural health monitoring are used to include additional auxiliary mass in the structure to change of natural frequencies. Therefore, the additional auxiliary mass can enhance the effects of discontinuities in the structural dynamics response, which could improve the identification and location of the discontinuities. The proposed approach deals with the wave propagation in structures regarding the spectral analysis method. The change in the natural frequencies due the mass is examined by comparing the differences between the dynamic responses of the beam with and without additional auxiliary mass. Similar analyses also performed with the Galerkin assumed modes technique to validate the new spectral element. The proposed technique is validated with numerical simulation and then compared to experimental data.

**Keywords** Spectral element method · Auxiliary mass spatial probing · Galerkin assumed modes technique.

E. U. L. Palechor · L. M. Bezerra
Civil Engineering Department, Faculty of Technology, University of Brasília,
Campus Universitário Darcy Ribeiro, Asa Norte, Brasília, DF 70910-900, Brazil
e-mail: erwinlopezpalechor@hotmail.com

L. M. Bezerra
e-mail: lmbz@unb.br

M. R. Machado (✉) · M. V. G. de Morais
Mechanical Engineering Department, Faculty of Technology, University of Brasília,
Campus Universitário Darcy Ribeiro, Asa Norte, Brasília, DF 70910-900, Brazil
e-mail: marcelam@unb.br

M. V. G. de Morais
e-mail: mvmorais@unb.br

# 1 Introduction

The spectral element method (SEM) consists in the exact displacement of the wave equation of the analytical solution in the frequency domain. It is equivalent to an infinite number of finite elements. SEM is a meshing method similar to FEM, where the approximated element shape functions are substituted by exact dynamic shape functions obtained from the exact solution of governing differential equations. As the SEM assumes the exact frequency-domain solution, it implies high accuracy. Other advantages of this method are the reduction of the problem size and DOFs, low computational costs, effectiveness in dealing with frequency-domain problems, adequate to deal with the non-reflecting boundary conditions of the infinite or semi-infinite-domain problems [11]. This characteristic and the spectral domain make SEM more suitable to solve the structural discontinues detection. The advantage of SEM is the reduced number of elements required to model the system as compared to other computational methods. Due to the SEM be formulated with the exact wave propagation solution, it became a suitable technique to model structural damage detection. In general, changes in either global or local structural properties can be associated with an imperfection or damage. In the last decades, damage detection researchers are focused on methods that use elastic wave propagation at medium and high-frequency bands [7, 8, 12, 14, 18, 20]. Some techniques in health structural monitoring use to add a traversing auxiliary mass change in the structure to enhance the effects of the discontinuities on the dynamic response and facilitate the identification and location, i.e., of damage. Zhong [21] presented damage detect technique that uses auxiliary mass spatial probing.

The modal analysis aims to reduce a complex system of partial differential equations that describe the dynamical behaviour of a continuous structure. This approach is less complicated and is described by a system of ordinary differential equations that considers the motion of an equivalent one-dimensional structure, such approach and numerical model especially in a non-linear analyses lead to errors in solution and must be treated with particular attention. Although the reduction of PDEs, especially non-linear systems analysis to ODEs and possibly algebraic equations to consideration of only a few degrees of freedom can lead to erroneous results. This approach in beam-like structure can be found in the references [2–4, 9]. A theoretical treatment of modal analysis is given in Meirovitch [13]. In literature, we found several examples of model reduction, for example, vortex induced vibration [5] or stochastic problems [17], or wind turbine analysis [16]. The order reduction can be made in the analysis. One of these techniques is to reduce the continuous system to a few degrees of freedom MDOF through modal analysis [1, 19]. Reducing continuous mechanical systems into discrete ones is advantageous. According to Galerkin's method [15].

The aim of this paper is to propose a new spectral element with additional mass. The proposed approach deals with the wave propagation in structures regarding the spectral analysis method. Methodologies for structural health monitoring are used to include additional auxiliary mass in the structure in order to change of natural frequencies. The change in the natural frequencies due the mass is examined by

comparing the differences between the dynamic responses of the beam with and without additional auxiliary mass. Similar analyse was also performed with the Galerkin assumed modes technique in order to validate the new spectral element with additional mass. The proposed model is validated with a numerical simulation and then compared to experimental data.

## 2 Beam Spectral Element with Additional Mass

A spectral damaged Euler-Bernoulli beam element with an auxiliary mass is addressed. Figure 1 shows a two-nodes auxiliary mass beam element with uniform rectangular cross-section, length $L$ and auxiliary mass position $L_1$. The auxiliary mass is modelled with a tip mass ($\vartheta \delta(x - L)$) added in the beam mass. The undamped equilibrium equation with the auxiliary mass in frequency domain can be written as:

$$EI\frac{d^4v(x)}{dx^4} + \omega^2[\rho A + \vartheta\delta(x - L)]v(x) = p(x), \tag{1}$$

where $I$ is the inertia moment, $v$ is the transverse displacement, and $p$ is the distributed external transversal force. A structural internal damping is introduced into the beam formulation as $EI = EI + c_{EI_0}$ with $c_{EI_0} = i\eta$ where $\eta$ is the hysteretic structural damping factor. The auxiliary mass is described by a impulse force described by a Dirac delta function ($\delta(x - L/2)$) multiplied by a mass value $\vartheta$. The homogeneous displacement solution for Eq. (1) must be described in two parts, one for the left-hand side of the mass, it has

$$v_L(x) = a_1 e^{-i(k_b x)} + a_2 e^{-(k_b x)} + a_3 e^{-ik_b(L_1 - x)} + a_4 e^{-k_b(L_1 - x)} \quad (0 \le x \le L_1)$$
$$= \mathbf{s}_L(x, \omega)\mathbf{a}_L \tag{2}$$

where $k_b = \sqrt{\omega}(\rho A/EI)^{1/4}$ is the beam wavenumber, $\mathbf{s}_L(x, \omega) = \left[e^{-i(k_b x)}\ e^{-(k_b x)}\ e^{-ik_b(L_1 - x)}\ e^{-k_b(L_1 - x)}\right]$, and $\mathbf{a}_L = \{a_1\ a_2\ a_3\ a_4\}^T$. Other, for the right-hand side of the mass

$$v_R(x) = a_5 e^{-ik_b(L_1 + x)} + a_6 e^{-k_b(L_1 + x)} + a_7 e^{-ik_b(L - (L_1 + x))}$$
$$+ a_8 e^{-k_b(L - (L_1 + x))} \quad (0 \le x \le L - L_1)$$
$$= \mathbf{s}_R(x, \omega)\mathbf{a}_R \tag{3}$$

where $\mathbf{s}_R(x, \omega) = \left[e^{-ik_b(L_1 + x)}\ e^{-k_b(L_1 + x)}\ e^{-ik_b(L - (L_1 + x))}\ e^{-k_b(L - (L_1 + x))}\right]$, and $\mathbf{a}_R = \{a_5\ a_6\ a_7\ a_8\}^T$. Writing Eqs. (2) and (3) in a matrix form,

$$\begin{Bmatrix} v_L(x) \\ v_R(x) \end{Bmatrix} = \mathbf{d} = \begin{bmatrix} \mathbf{s}_L(x, \omega) & \mathbf{0} \\ \mathbf{0} & \mathbf{s}_R(x, \omega) \end{bmatrix} \begin{Bmatrix} \mathbf{a}_L \\ \mathbf{a}_R \end{Bmatrix} = \mathbf{s}(x, \omega)\mathbf{a} \tag{4}$$
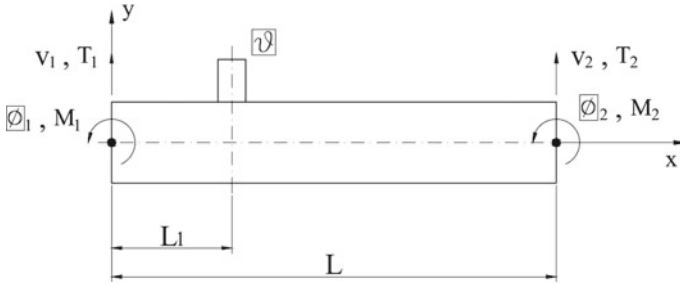
**Fig. 1** Two-node damaged beam spectral element

where $\mathbf{d}$ is the nodal displacement vector, $\mathbf{a}$ is the coefficient vector, and $\mathbf{s}$ is a matrix dependent of the element boundary and compatibility conditions. The element boundary conditions are considered as following form:

- at node 1

$$v_L(0) = v_1 \quad \text{and} \quad \frac{\partial v_L(0)}{\partial x} = \phi_1 \tag{5}$$

- at the mass location ($x = L_1$ for $v_L(x)$ and $x = 0$ for $v_R(x)$)

$$
\begin{aligned}
v_L(L_1) &= v_R(0), \\
\frac{\partial v_L(L_1)}{\partial x} &= \frac{\partial v_R(0)}{\partial x}, \\
\frac{\partial^2 v_L(L_1)}{\partial x^2} &= \frac{\partial^2 v_R(0)}{\partial x^2}, \\
\frac{\partial^3 v_L(L_1)}{\partial x^3} - \frac{\partial^3 v_R(0)}{\partial x^3} &= -\vartheta \frac{\partial^2 v_L(L_1)}{\partial t^2}
\end{aligned}
\tag{6}
$$

- at node 2

$$v_R(L - L_1) = v_2 \quad \text{and} \quad \frac{\partial v_R(L - L_1)}{\partial x} = \phi_2 \tag{7}$$

Applying boundary and compatibility conditions in Eq. (4) it has,

$$
\underbrace{\begin{bmatrix}
1 & 1 & m & n & 0 & 0 & 0 & 0 \\
-ik & -k & ik\mathsf{m} & k\mathsf{n} & 0 & 0 & 0 & 0 \\
-m & -n & 1 & 1 & \mathsf{m} & \mathsf{n} & \mathsf{o} & \mathsf{p} \\
mik & nk & -ik & -k & -ik\mathsf{m} & -k\mathsf{n} & ik\mathsf{o} & k\mathsf{p} \\
-k^2m & k^2n & -k^2 & k^2 & k^2\mathsf{m} & -k^2\mathsf{n} & k^2\mathsf{o} & -k^2\mathsf{p} \\
ik^3m + \vartheta ik^2m & -k^3n + \vartheta k^2 & -ik^3 + \vartheta ik^2 & k^3 + \vartheta k^2 & -k^3\mathsf{m} & k^3\mathsf{nn} & ik^3\mathsf{o} & -k^3\mathsf{p} \\
0 & 0 & 0 & 0 & \mathsf{r} & \mathsf{t} & 1 & 1 \\
0 & 0 & 0 & 0 & -ik\mathsf{r} & -k\mathsf{t} & ik & k
\end{bmatrix}}_{\mathbf{G}_b}
\begin{Bmatrix}
a_1 \\ a_2 \\ a_3 \\ a_4 \\ a_5 \\ a_6 \\ a_7 \\ a_8
\end{Bmatrix}
=
\begin{Bmatrix}
v_1 \\ \phi_1 \\ 0 \\ 0 \\ 0 \\ 0 \\ v_2 \\ \phi_2
\end{Bmatrix}
$$

$$\tag{8}$$

where $\mathsf{m} = e^{ikL_1}$, $\mathsf{n} = e^{-kL_1}$, $\mathsf{o} = e^{-ik(L-L_1)}$, $\mathsf{p} = e^{k(L-L_1)}$, $\mathsf{r} = e^{-ikL}$, $\mathsf{t} = e^{-kL}$. From the Eq. (8) it can relate the coefficient vector with the nodal displacement vector by:

$$\mathbf{a} = \mathbf{G}_{br}^{-1}\mathbf{d} \tag{9}$$

where $\mathbf{G}_{br}^{-1}$ is the inverse of $\mathbf{G}_b$ reduced to the order $[8 \times 4]$ due to the zeros into the displacement vector $\mathbf{d}$. Substituting Eq. (9) into (4) it has,

$$\left\{ \begin{array}{c} v_L(x) \\ v_R(x) \end{array} \right\} = \left[ \begin{array}{cc} \mathbf{s}_L(x, \omega) & \mathbf{0} \\ \mathbf{0} & \mathbf{s}_R(x, \omega) \end{array} \right] \mathbf{G}_{br}^{-1}\mathbf{d} = \mathbf{g}(x, \omega)\mathbf{d} \tag{10}$$

Note that $\Gamma(\omega) = \mathbf{G}_{br}^{-1}$. For instance the deterministic flexibility rigidity and mass per unit of length parameters, $EI(x)$ and $\rho A(x)$, are assumed as deterministic constants. The stiffness operator is given by $\partial^2(\bullet)/\partial x^2 = (\bullet)''$. Due spacial reference in the model the equations must be integrated according to the corresponding limits, then

$$\mathbf{K}(\omega) = EI\Gamma_d^T(\omega) \left[ \begin{array}{cc} \mathbf{Sk}_{0L} & \mathbf{0} \\ \mathbf{0} & \mathbf{Sk}_{0R} \end{array} \right] \Gamma(\omega), \tag{11}$$

and

$$\mathbf{M}(\omega) = \rho A \; \Gamma_d^T(\omega) \left[ \begin{array}{cc} \mathbf{Sm}_{0L} & \mathbf{0} \\ \mathbf{0} & \mathbf{Sm}_{0R} \end{array} \right] \Gamma(\omega), \tag{12}$$

where

$$\mathbf{Sk}_{0L} = \int_0^{L_1} \mathbf{s}''^T_L(x, \omega)\mathbf{s}''_L(x, \omega)dx, \qquad \mathbf{Sk}_{0R} = \int_0^{(L-L_1)} \mathbf{s}''^T_R(x, \omega)\mathbf{s}''_R(x, \omega)dx \tag{13}$$

$$\mathbf{Sm}_{0L} = \int_0^{L_1} \mathbf{s}^T_L(x, \omega)\mathbf{s}_L(x, \omega)dx, \qquad \mathbf{Sm}_{0R} = \int_0^{(L-L_1)} \mathbf{s}^T_R(x, \omega)\mathbf{s}_R(x, \omega)dx \tag{14}$$

Substituting Eqs. (13) in (11), and Eqs. (14) in (12) the deterministic stiffness and mass matrices as closed-form expressions can be obtained. Then, the spectral beam with auxiliary dynamic stiffness matrix can be obtained as $\mathbf{D}(\omega) = \mathbf{K}(\omega)\omega^2\mathbf{M}(\omega)$.

## 3   Experimental Procedure

Experimental results are performed for a I-beam $102 \times 11.4$ (exact dimensions $101.6 \times 67.6$ mm$^2$) of steel MR-250 with length of 6 m. Figure 2   show in detail the nominal geometric properties of I-beam. The Young's modulus is $E = 200.0474 \pm 2.0675$ (nominal 200) GPa, cross-sectional area $A = 14.3156$ cm$^2$, density $\rho = 7848.156$ kg/m$^3$ and moment of inertia $I_x = 245.13$ cm$^4$ were obtained

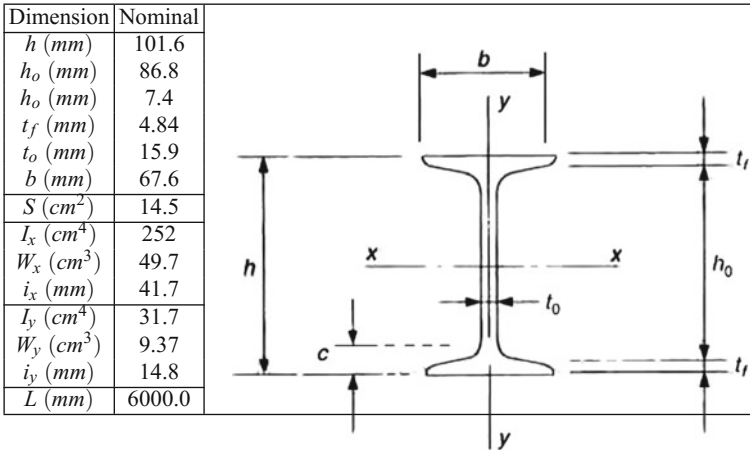| Dimension | Nominal |
|-----------|---------|
| $h\ (mm)$ | 101.6 |
| $h_o\ (mm)$ | 86.8 |
| $h_o\ (mm)$ | 7.4 |
| $t_f\ (mm)$ | 4.84 |
| $t_o\ (mm)$ | 15.9 |
| $b\ (mm)$ | 67.6 |
| $S\ (cm^2)$ | 14.5 |
| $I_x\ (cm^4)$ | 252 |
| $W_x\ (cm^3)$ | 49.7 |
| $i_x\ (mm)$ | 41.7 |
| $I_y\ (cm^4)$ | 31.7 |
| $W_y\ (cm^3)$ | 9.37 |
| $i_y\ (mm)$ | 14.8 |
| $L\ (mm)$ | 6000.0 |

**Fig. 2** Geometrical properties of I-shape $102 \times 11.4$
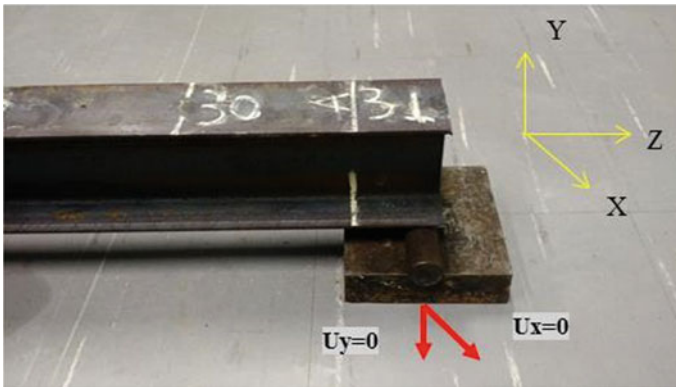


**Fig. 3** Simply supported condition at both ends

experimentally. The dynamic tests were developed in laboratory of Mechanical Engineering Department of University of Braslia.

Geometric properties (area $A$ and inertia $I_x$) was determined by articulated arm coordinate measuring machine (model Arm100 - uncertainty of 0.070 mm) of Metrology Laboratory (UnB-FT/EnM/LabMetro). With Archimedes principle, we obtain an density estimation of material. The experimental verification of Young modulus was performed by FRF estimation of a free-free and simply supported Euler-Bernoulli beam. With a modal impact testing, Young modulus was estimated by report to the best fit to natural frequencies identified. The tested beam has simply supported condition guarantee by steel rollers lean on steel plates, as show by Fig. 3.
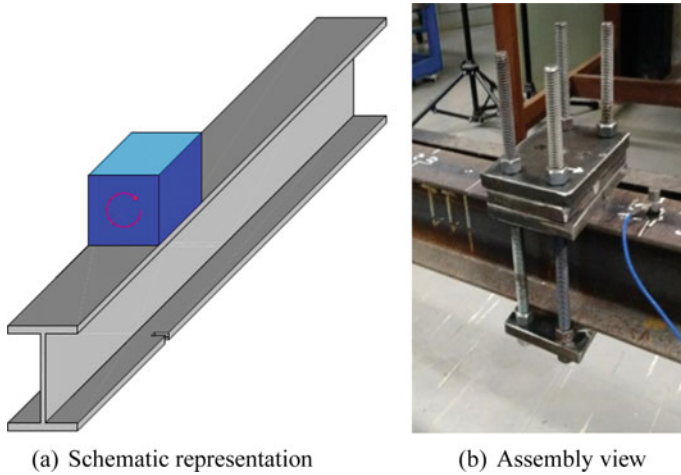
(a) Schematic representation      (b) Assembly view

**Fig. 4** Additional mass

The additional mass was composed by steel plates fixed with four threaded rod and nuts as shown in Fig. 4. Each steel plate weighted $5714 \pm 2g$. The added mass system was fast to avoid any accidental motion.

**Instrumentation and Experimental Procedure**

Figure 5 describe experimental setup in Laboratory of Vibration in University of Braslia to estimate FRF between modal hammer and accelerometer. The list of equipments are NI cDAQ-91 and NI-9124, accelerometers PCB352C34/PCB352C33, modal hammer PCB086C0, and a PC desktop with LabView to data acquisition. For experimental tests, one accelerometers located in $L/4$ from the right support and an impact in force in the $L/4$ from the right support.

The additional mass was placed along the beam every 20 cm. Once the masses were positioned, the modal hammer tests were performed to obtain the FRFs. The first and second frequencies for each position of the additional mass were identified by spectral centre correction method [21] (Table 1).

## 4 Numerical Results

In the first numerical example, a simply supported beam boundary conditions with the same material properties and geometry presented in Sect. 3. The impact and measured points are also assumed likewise in the experimental test setup. It is compared the firsts natural frequencies of the beam with and without auxiliary mass spatial probing. In Fig. 6 shows that when no mass is added to the structure the first natural frequency is constant, while that the beam with additional mass the first natural frequency
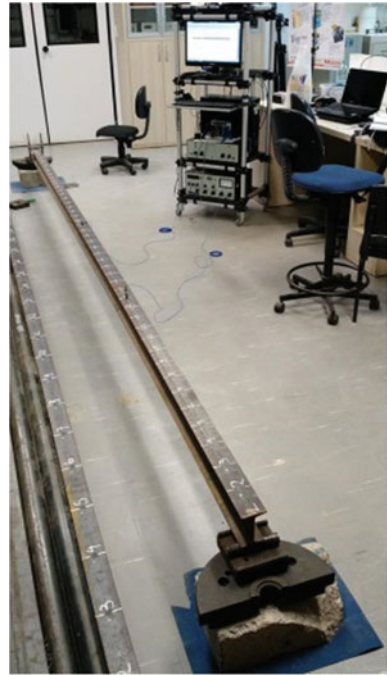
**Fig. 5** General view of
experimental setup



**Table 1** First and second frequency (Hz) as function of position of additional mass (cm)

| $x$(cm) | 0.0 | 0.2 | 0.4 | 0.6 | 0.8 | 1.0 | 1.2 | 1.4 | 1.6 | 1.8 |
|---|---|---|---|---|---|---|---|---|---|---|
| $f_1$ | 9.329 | 9.336 | 9.320 | 9.270 | 9.219 | 9.168 | 9.106 | 9.034 | 8.956 | 8.893 |
| $f_2$ | 36.804 | 36.719 | 36.501 | 36.211 | 35.890 | 35.593 | 35.392 | 35.281 | 35.300 | 35.432 |
| $x$(cm) | 2.0 | 2.2 | 2.4 | 2.6 | 2.8 | 3.0 | 3.2 | 3.4 | 3.6 | 3.8 |
| $f_1$ | 8.836 | 8.793 | 8.746 | 8.709 | 8.694 | 8.683 | 8.686 | 8.711 | 8.747 | 8.792 |
| $f_2$ | 35.656 | 35.940 | 36.249 | 36.517 | 36.709 | 36.794 | 36.728 | 36.539 | 36.278 | 35.975 |
| $x$(cm) | 4.0 | 4.2 | 4.4 | 4.6 | 4.8 | 5.0 | 5.2 | 5.4 | 5.6 | 5.8 |
| $f_1$ | 8.838 | 8.900 | 8.964 | 9.031 | 9.100 | 9.167 | 9.224 | 9.263 | 9.298 | 9.327 |
| $f_2$ | 35.685 | 35.448 | 35.310 | 35.278 | 35.373 | 35.578 | 35.871 | 36.192 | 36.489 | 36.694 |

change when the auxiliary mass change position. The additional auxiliary mass
approximately 10% of the beam mass ($\vartheta = 0.54$ kg).

For the second example compare the firsts frequencies obtained with the SEM
model, Galerkin [1] and experimental measured. Figure 7 presents experimental
results and SEM simulation of accelerometer 2 ($x = L/4$) FRF with additional mass
at middle span. This figure compare experimental results and SEM simulation with
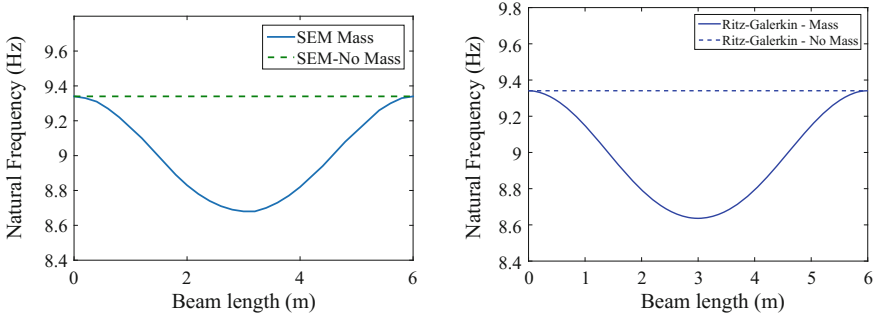a reasonable agreement. The error are more notable to second frequency.

**Fig. 6** First frequency as function of position of additional mass obtained using the SEM and Ritz-Galerkin with and without auxiliary added mass
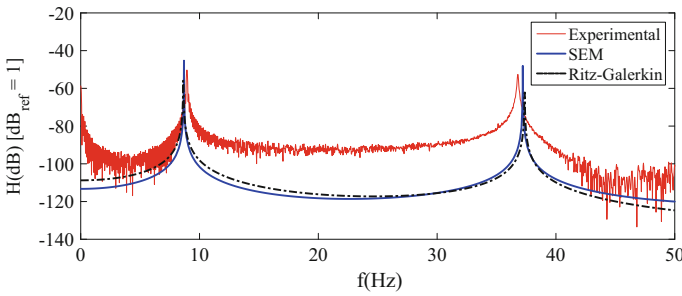


**Fig. 7** FRF of accelerometer 2 ($x = L/4$) with additional mass at middle span: comparison of SEM, Ritz-Galerkin and experimental results
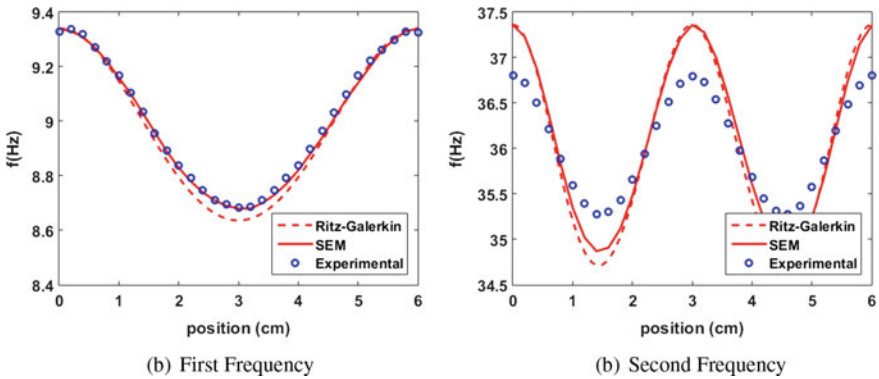


(b) First Frequency

(b) Second Frequency

**Fig. 8** Natural frequencies of beam $f_i (i = 1, 2)$[Hz] as function of additional mass $x$[cm]

Figure 8 show the first two natural frequency of essayed beam as function of addition mass position $x$[cm]. The error between SEM simulation and experimental are inferior of 1.2%.

## 5   Conclusions

This paper present a new spectral element with additional mass. The natural frequencies change due to position of the mass along x-axis. Similar analyse was also performed with the Galerkin assumed modes technique in order to validate the new spectral element with additional mass. Galerkin technique presents similar results to spectral element method even needing some assumed modes to converge ($N \geq 6$).

The proposed model is validated with a numerical simulation and then compared to experimental data. The spectral element results shows a good agreement with experimental first natural frequencies. Comparing the second natural frequencies experimentally identified, the spectral element observe a difference inferior to 1.2%.

## Appendix

According to Galerkin's method [15], the solution of Eq. (1) can be expanded as function of:

$$w(x, t) \cong w_h(x, t) = \sum_{j=1}^{N} \psi_j(x) \, q_j(t) \tag{15}$$

where $\psi_j(x)$ are test functions in domain $\mathbb{D} = [0, L]$ that satisfying boundary conditions of problem, $q_j(t)$ are generalized coordinates of discretized system. By substituting (15) into (1) to obtain residual function $\mathscr{R}$. As base functions are not exact solutions of problem (1), the residual function $\mathscr{R}$ results a non-null function. But, according to Garlerkin's method, a kind of weighted residual method [6, 10], we search minimize the residual function $\mathscr{R}$ in domain $\mathscr{D} \in [0, L]$,

$$\int_{\mathscr{D}} \mathscr{R}\left[w_h(x, t)\right] \cdot \psi_i(x) dx = 0, \qquad i = 1, 2, \ldots, N \tag{16}$$

This problem can be solved by a numerical time integrator, e.g., Newmark method, Hilbert-Hughes-Taylor method, or a simple Runge-Kutta.

## References

1. Avila, S.M., Shzu, M.A.M., Pereira, W.M., Santos, L.S., Morais, M.V.G., Prado, Z.J.G.: Numerical modeling of the dynamic behavior of a wind turbine tower. J. Vibr. Eng. Technol. **4**(3), 249–257 (2016)

2. Awrejcewicz, J., Krysko, A.V., Kutepov, I.E., Zagniboroda, N.A., Dobriyan, V., Krysko, V.A.: Chaotic dynamics of flexible Euler-Bernoulli beams. Chaos: an Interdisciplinary. J. Nonlinear Sci. **23**(4), 36–43 (2013)
3. Awrejcewicz, J., Krysko, A.V., Mrozowski, J., Saltykova, O.A., Zhigalov, M.V.: Analysis of regular and chaotic dynamics of the Euler-Bernoulli beams using finite difference and finite element methods. Acta. Mech. Sin. **27**(1), 36–43 (2011)
4. Awrejcewicz, J., Saltykova, O.A., Zhigalov, M.V.: Analysis of non-linear vibrations of single-layered Euler-Bonoulli beams using wavelets. Int. J. Aerosp. Lightweight Struct. **1**(2), 203–219 (2011)
5. Blevins, R.: Flow-Induced Vibration. Krieger Publishing Company, New York (2001)
6. Finlayson, B.A., Scriven, L.E.: The Method of Weighted Residuals - A Review (1966)
7. Krawczuk, M.: Application of spectral beam finite element with a crack and iterative search technique for damage detection. Finite Elem. Anal. Des. **80**, 1809–1816 (2002)
8. Krawczuk, M., Grabowska, J., Palacz, M.: Longitudinal wave propagation. Part I- comparison of rod theories. J. Sound Vib. **295**, 461–478 (2006)
9. Krysko, V.A., Awrejcewicz, J.: On the vibration of the Euler-Bernoulli beam with clamped ends deflection constraints. Int. J. Bifurcat. Chaos **15**(6), 1867–1878 (2005)
10. Kwon, Y.W., Bang, H.: The Finite Element Method Using Matlab. CRC Press, Boca Raton, FL (2000)
11. Lee, U.: Spectral Element Method in Structural Dynamics. Inha University Press, Incheon (2004)
12. Machado, M.R., Santos, J.M.C.D.: Reliability analysis of damaged beam spectral element with parameter uncertainties. Shock Vib. **2015** (2015) 12 p
13. Meirovitch, L.: Analytical Methods in Vibrations. Macmillan, New York (1967)
14. Ostachowicz, W.M.: Damage detection of structures using spectral finite element method. Comput. Struct. **86**, 454–462 (2008)
15. Paidoussis, M.P.: Fluid Structure Interactions. Slender Structures and Axial Flow, vol. 1. Elsevier Academic Press, Amsterdam (1998)
16. Peeters, J.L., Vandepitte, D., Sas, P.: Analysis of internal drive train dynamics in a wind turbine pp. 141–161
17. Ritto, T.G., Sampaio, R., Cataldo, E.: Timoshenko beam with uncertainty on the boundary conditions. J. Braz. Soc. Mech. Sci. Eng. **30**(4), 295–303 (2008)
18. Santos, E., Arruda, J., Santos, J.D.: Modeling of coupled structural systems by an energy spectral element method. J. Sound Vib. **36**, 1–24 (2008)
19. Soong, T.T., Dargush, G.F.: Passive Energy Dissipation Systems in Structural Engineering. Wiley, New York (1997)
20. Su, Z., Ye, L.: Identification of Damage Using Lamb Waves. Springer, Berlin (2009)
21. Zhong, S., Oyadiji, S.O., Ding, K.: Response-only method for damage detection of beam-like structures using high accuracy frequencies with auxiliary mass spatial probing. J. Sound Vib. **311**, 1075–1099 (2008)